Marine Mammal Science

MARINE MAMMAL SCIENCE, 28(4): 690–713 (October 2012)

DOI: 10.1111/j.1748-7692.2011.00526.x

Morphology of the odontocete melon and its implications for acoustic function

MEGAN F. MCKENNA
Scripps Institution of Oceanography,
University of California San Diego,
9500 Gilman Drive, Mail Code 0205,
La Jolla, California 92093-0208, U.S.A.
E-mail: megan.mckenna@gmail.com

TED W. CRANFORD
ANNALISA BERTA
Department of Biology,
San Diego State University,
San Diego, California 92182-4614, U.S.A.

NICHOLAS D. PYENSON
Department of Paleobiology,
National Museum of Natural History,
Smithsonian Institution,
PO Box 37012,
Washington, DC 20013-7013, U.S.A.
and
Departments of Mammalogy and Paleontology,
Burke Museum of Natural History and Culture,
Seattle, Washington 98195, U.S.A.

ABSTRACT

Toothed whales (crown Odontoceti) are unique among mammals in their ability to echolocate underwater, using specialized tissue structures. The melon, a structure composed of fat and connective tissue, is an important component in the production of an echolocation beam; it is known to focus high frequency, short duration echolocation clicks. Here, we report on the morphology of the odontocete melon to provide a comprehensive understanding of melon structure across odontocete taxa. This study examined nine odontocete species (12 individual specimens), from five of the ten extant odontocete families. We established standardized definitions using computed tomography scans of the melon to investigate structure without losing geometric integrity. The morphological features that relate to the focusing capacity of the melon include internal density topography, melon size and shape, and relationship to other forehead structures. The potential for melon structure to act as a filter is discussed: establishing a lower limit to the frequency of sounds that can be propagated through the head. Collectively, the results of this study provide a robust, quantitative and comparative framework for evaluating tissue structures that form a key component of the echolocation apparatus.

Key words: odontocetes, sound production, echolocation, melon, functional morphology, computed tomography.

Odontocetes (toothed whales) are one of the two surviving lineages of marine mammals that descended from terrestrial artiodactyls approximately 55 mya and evolved numerous adaptations for life in an aquatic environment (reviewed by Fordyce and Muizon 2001, Gingerich 2005). Among these traits is the ability to produce underwater high-frequency, short-duration sounds, and to detect and interpret the returning echo, a behavior known as echolocation (Griffin 1980, Au 1993). Odontocetes have a sophisticated underwater echolocation system that requires a unique suite of anatomic features (Lawerence and Schevill 1956; Norris 1969; Norris and Harvey 1974; Mead 1975; Heyning 1989; Heyning and Mead 1990; Cranford 1992; Cranford *et al.* 1996, 2008*b*; Harper *et al.* 2008; Huggenberger *et al.* 2008, 2009), which allow them to successfully exploit resources and communicate in the marine environment (Lindberg and Pyenson 2007).

The anatomy associated with the production of echolocation clicks is complex and does not share any homologues with other echolocating mammals (*e.g.*, microchiropteran bats, and soricid and tenrecid shrews) (Neuweiler 2000, Thomas and Jalili 2003). Click generation in toothed whales is hypothesized to begin by action of the palatopharyngeal muscle complex, which initially pulls the larynx dorsally, into the inferior bony nares and pressurizes the air in the bony nasal passages (Cranford *et al.* 1996, in press). The pressurized air passes through the phonic lips formed by two bilateral, narrow slits that define the dorsal end of the spiracular cavity, causing vibrations in the adjacent ellipsoid fat bodies (*i.e.,* dorsal bursae). These vibrations are reflected anteriorly by the skull, a collection of nasal air sacs, and a dense connective tissue theca that function together as a concave acoustic mirror, along with the fat bodies near the vertex of this megaphone-like structure (Fig. 1). Sound vibrations propagate along multiple pathways through the melon and emerge into the environment (Aroyan *et al.* 1992, Cranford *et al.* 2008*a*) as a click that may be tens of microseconds to milliseconds in duration depending on the species (Au 1993). The odontocete melon (homologous to the junk in sperm whales; Cranford 1999) is a unique specialized organ within the enlarged nasal apparatus. The melon is composed mainly of fat and connective tissue fibers (Harper *et al.* 2008). The tissue properties of the melon are thought to focus sound energy generated in the bursae complex and decrease acoustic attenuation at the tissue-water interface by impedance matching (Norris and Harvey 1974, Amundin and Andersen 1983, Au *et al.* 2006, Cranford *et al.* 2008*a*).

Although the melon is an important component of the echolocation system, previous studies have not quantitatively defined its structure in a diverse array of species, thereby eliminating the comparative power in evaluating the morphological and functional differences across the Odontoceti (Cranford *et al.* 1996, McKenna 2005, McKenna *et al.* 2007, Harper *et al.* 2008). This challenge can be partially attributed to the melon's graded characteristic. At normal mammalian body temperatures, the melon is a lipid and connective tissue structure marked by changing density gradients, from a shell composed largely of a collagen fiber mesh to a fluid-like core rich in specialized lipids. The geometric relationships between the melon and nearby structures are necessarily sacrificed during conventional gross dissections. Furthermore, defining the melon is complicated because it protrudes through a structure of

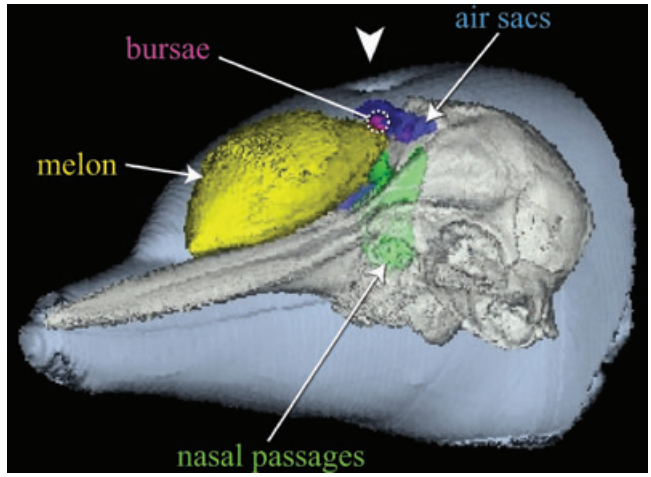

Figure 1. Three-dimensional reconstruction of the sound production tissues in the head of *T. truncatus*, in anterolateral view. Shown are the melon (yellow), the bursae (magenta), air sacs (blue), and the nasal passages (green). Skull is highlighted in light blue against the slightly darker blue representing the external morphology of the head. The white arrowhead indicates the external blowhole. The theca is not pictured because it obstructs the view of the features listed earlier.

similar density, the blubber, a lipid-infused blanket that covers much of the body and portions of the head. In this study, these fundamental hurdles were surmounted by using X-ray computed tomography (CT) and image processing tools to define the melon boundaries, without perturbing the *in situ* geometry by dissection. We generated a standardized definition for melon boundaries from the CT scans, and achieved quantitative and qualitative comparisons of melon morphology across the Odontoceti.

Odontocete echolocation involves an array of anatomic components used to generate, propagate, and receive sounds. Understanding these system functions requires detailed study of anatomic geometry. Our intricate investigations of the cephalic morphology can be combined with measurements of tissue properties to produce computerized models and simulations of odontocete echolocation anatomy. Recent studies have simulated echolocation beam formation from the heads of toothed whales (Aroyan *et al*. 1992, Cranford *et al.* 2008*a*). Results from these computer simulations are analytically powerful and can provide valuable insights into the mechanisms of sound production, beam formation, and sound reception. However, these studies are often limited to single specimens of a few species, thereby limiting the interpretive power that could be gleaned from comparisons across a broad spectrum of odontocete species. This is a substantial limitation given the complex morphological diversity in cephalic anatomy across odontocetes (Schenkkan and Purves 1973, Cranford *et al.* 1996); making it difficult to apply the specific modeling results across species. By combining our quantitative definition of the melon with previously reported experimental research, functional hypotheses can be tentatively extrapolated to include relatively unknown species.

This study defines and quantifies melon morphology across a diverse spectrum of odontocetes. Results are presented for five of the ten extant odontocete families. The

implications for acoustic function are discussed based on the observed differences in structure, strengthening previous work that highlights the focusing capability of the melon. An additional function of the melon (*i.e.,* establishing a lower limit to the frequency of the sound projected into a beam from the head) is also examined and the morphological components that pertain to this function are described.

Materials and Methods

Represented Taxa

This study included nine odontocete species (totaling 12 individual postmortem specimens). Five of the ten extant families of odontocetes were represented: Kogiidae (1 species), Ziphiidae (1 species), Pontoporiidae (1 species), Delphinidae (5 species), and Phocoenidae (1 species) (Table 1). Even though the specimens scanned for this study represent a subset of the 76 extant odontocete species, the strength of this study emerges from the comparisons across odontocete families using a few representative species, allowing us to detect broad outlines in morphological patterns.

CT Scanning Instrumentation and Protocol

CT data were acquired from three sources: (1) an unpublished library of previously collected scans using a medical scanner (Cranford *et al.* 1996; including *Kogia breviceps, Pontoporia blainvillei, Lagenorhynchus obliquidens, Delphinus delphis, Tursiops truncatus,* and *Phocoena phocoena*); (2) medical CT scans from current related studies (for a neonate *Ziphius cavirostris* and *Steno bredanensis*); and (3) an industrial CT scanner (for an adult *Z. cavirostris* and *Orcinus orca*).

Precautions were taken in specimen preparation to ensure freshness of the material; therefore the morphological descriptions of postmortem material, based on CT scanning, provided the closest approximation to live tissues we could achieve (McKenna *et al.* 2007). To avoid significant tissue decomposition, we placed the heads in a freezer as soon after death as possible, often within a few hours. Before scanning at medical imaging facilities, we thawed the heads in a water bath to ensure rapid, thorough, and uniform tissue thawing. We then wrapped the heads in several layers of plastic and, whenever possible, placed them in a registration frame in order to hold specimens in a common orientation and provide a density phantom for calibration purposes (see Cranford *et al.* 1996 for description of the procedure). We used an industrial CT scanner for specimens too large for the medical scanner. The protocol used for these specimens differed from that for the medical scanner in that the heads scanned with industrial CT remained frozen, and we incased these heads in cardboard and foam, along with density calibration rods, to maintain a consistent orientation (Cranford *et al.* 2008*a*, *b*).

We compiled and processed the CT data for all specimens using image processing software, Analyze (ver. 5.0 and 6.0) (Robb and Barillot 1989, Robb *et al.* 1989, Robb 1999). Each 2-D scan consists of a matrix of values (*i.e.,* CT numbers) expressing linear attenuation of X-rays by the material (tissue) at a specific geometric location. The CT numbers are calibrated to the Hounsfield scale (−1,000 to 1,000) and presented as Hounsfield units (HUs) (Robb 1999). The HU is a calibrated measure of electron density and is equivalent to the change in density of 1 cm^3 of water as temperature increases 1°C (Robb 1999), at standard temperature and pressure. These

Table 1. Quantitative descriptions of the odontocete melon anatomy (*skull is not complete, no measurements).

	Kogiidae	Ziphiidae		Pontoporiidae	Delphinidae							Phocoenidae
Morphological characters	*Kogia breviceps*	*Ziphius cavirostris*	*Ziphius cavirostris*	*Pontoporia blainvillei*	*Lagenorhynchus obliquidens*	*Steno bredanensis*	*Delphinus delphis*	*Tursiops truncatus*	*Tursiops truncatus*	*Tursiops truncatus*	*Orcinus orca*	*Phocoena phocoena*
Life history												
Age class	juvenile	adult	neonate	juvenile	adult	adult	adult	adult	adult	adult	adult	adult
Sex	male	male	female	female	female	female	male	male	male	female	female	male
Body length (cm)	163.0	515.0	314.9	130.0	–	228	189.0	238.8	238.0	–	671.0	156.6
Size												
Head length (cm)	11.1	142.3	32.7	2.0	7.4	15.6	10.2	14.5	*	11.6	346.9	4.8
Melon length (cm)	0.7	2.3	1.0	0.1	0.2	0.3	0.3	0.6	0.6	0.6	7.6	0.1
Percent of head volume	6.7	1.6	2.9	6.0	2.8	2.1	3.1	3.9	*	5.4	2.2	2.5
Melon length (cm)	15.0	24.8	25.6	10.2	14.4	14.1	15.5	19.6	19.4	19.1	46.0	11.7
Condylobasal length (cm)	25.0	84.7	51.6	31.0	35.5	50.5	43.5	46.0	*	45.5	94.5	27.2
Percent of head length	60.0	29.3	49.6	32.9	40.6	27.9	35.6	42.6	*	41.9	48.7	43.0
Topography												
Mean HU (±SD)	−82.7 (12.0)	frozen	−56.5 (13.2)	−74.7 (11.6)	−57.9 (8.8)	−50 (1.3)	−58.6 (12.1)	−81.0 (4.3)	−89.2 (3.1)	−91.4 (3.8)	frozen	−66.2 (8.9)
Range HU	80	frozen	84	169	50	6	103	94	68	60	frozen	59
Geometric												
Width of aperture (cm)	2.4	19.6	12.9	2	2.5	3.3	3.8	5.4	5.1	5.9	22.9	3.8

Hounsfield values comprise the CT images and are tightly correlated with density, an important characteristic that partially determines sound speed in any material. The elastic property, or Young's modulus, of tissue is the other primary component that determines sound speed (Soldevilla *et al.* 2005). When density is mentioned in this paper, it is shorthand for the electron density contained within the calculation of HU and for our purposes is understood to be, essentially, the density of the tissue (Soldevilla *et al.* 2005, Cranford *et al.* 2008*b*).

Anatomical Segmentation and Morphological Measurements

We selected measurements for this study based on the likelihood that they are important to the acoustic functions of the melon (*i.e.,* focusing capability and impedance matching). The accuracy of the measurements depends, to some degree, on the ability of the operator to interpret structure from images based on density differences. We used established protocols to inform such interpretive decisions (see McKenna 2005 and table 2 in Cranford *et al.* 2008*b*).

X-ray CT was a valuable tool for visualizing the undisturbed geometric relationships between tissues and organs. Using CT data and our image processing protocols in Analyze, it was possible to discern morphological features by "segmentation." Segmentation is the process of defining the boundaries of structures by differences in X-ray attenuation (*i.e.,* density), based on the ability of the human operator to discriminate changes in gray scale (or hues in color images). The process of segmentation included several protocols that facilitate choosing these boundaries consistently based on quantifiable differences in density; the greater the difference, the easier it is to separate structures from one another along common boundaries. For example, the boundary between bone and air is easily discernable in the CT scans; however, the boundaries between soft tissue structures with similar densities are more difficult to discriminate.

The melon is composed of differing proportions of lipids and connective tissue (Harper *et al.* 2008). In the CT scans, the boundaries of the melon are represented by gradients in density, from a lower density core, composed largely of lipids, to higher density shell invested by increasing proportions of connective tissue. The CT scans presented here, show a break in the slope of that gradient from the outer shell of the melon to its low density core. For the purpose of this analysis, we defined the outer melon boundaries quantitatively in the following manner. First, we selected a homologous transverse slice through the posterior border of the antorbital notch, a homologous landmark on the skulls of all examined specimens. Within this slice, a horizontal (*i.e.,* right to left) line was drawn across the (dorsoventral) middle of the melon in each specimen (represented by the white dashed line in Fig. 2A). The middle was defined as half way between the dorsal surface of the head in that slice and the dorsal aspect of the bones that comprise the antorbital notch (lacrimojugal, maxilla, and frontal bones; according to Mead and Fordyce 2009). We plotted the HU values along this line (every 1.5 mm). The outer boundaries of the melon were determined to be a gradient of 10 HU or greater between adjacent points in the profile (Fig. 2B). The 10 HU difference gradient was chosen as the standard definition of the melon boundary. This standard gradient could be located in all specimens examined. Comparing the location of the outer gradient with dissected specimens confirms that this scan-based boundary agrees with the transition from largely connective tissue or muscle components to the mixed fat and connective tissues of the melon. Because the

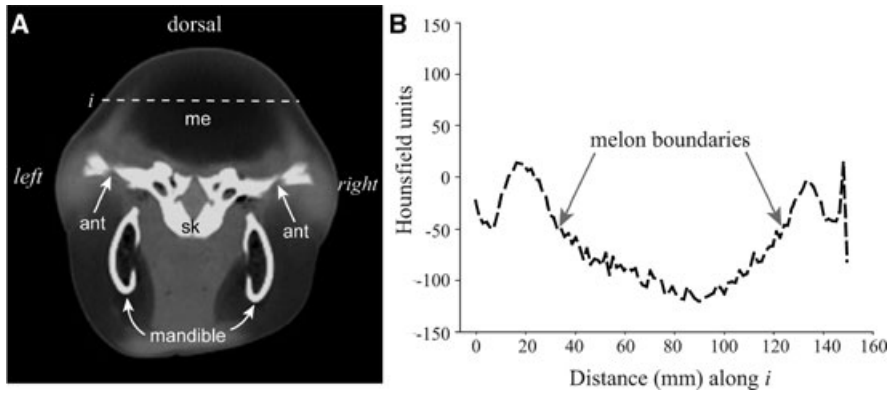

Figure 2. Definition of melon boundaries, using CT scan of *T. truncatus*, based on change in Hounsfield units (HU). (A) Transverse tomographic reconstruction at the antorbital notches near the supraorbital process of the frontal bones. The dashed line *i* shows the location of the line profile displayed in (B). Abbreviations: me = melon, sk = skull, ant = antorbital notch of the frontal bone. (B) Graph of line profile showing the change in density along the dashed line *i* in (A). The y-axis represents the change in HUs plotted over a specified distance (mm) along the dashed line *i* in (A). The melon boundaries defined by a change in 10 HU at adjacent locations are indicated by the gray arrows.

dimensions of the pixels in each scan were the same (1.5 mm) across all specimens, we defined the melon boundaries based on a slope greater than or equal to 6.67 (*i.e.,* 10 HU/1.5 mm). We then applied this defined boundary based on a range of HU values to all the slices of the head—both anterior and posterior to the transverse slice at the antorbital notch. The melon boundary intersected the surface of the forehead anteriorly. Where this occurred, we defined the boundary of the melon to a layer of pixels just below the surface of the forehead.

The boundaries at the external surface of the head (*i.e.*, the skin), the skull, and nasal passages were all determined by a threshold operation, an automated image processing technique used to select a specific range of HU values. This approach was possible when there was a substantial difference in density between the structure of interest and the surrounding tissue. We manually segmented the small elliptical lipid dorsal bursae from the surrounding anatomy because these structures are thought to be the sources for echolocation signals.

Quantitative Melon Measurements

Once we segmented or "defined" the boundaries for the structures of interest, we made measurements of various quantities related to the melon, including its size, shape, density, internal structure, and the geometric relationships to other structures of the head (*i.e.,* the surface of the head and the bursae). The specific measurements (which are defined later) were intended to highlight quantities with the potential for functional implications. The specific melon functions and morphological features of interest are: (1) biosonar beam formation and the potential for focusing (by refraction or reflection or constructive and destructive interference), for which we describe density topography, relative size of the melon, and melon shape; (2) potential

pathways for sound transmission in the head, for which we considered the nature of the connection between the melon and the bursae (*i.e.,* sound sources), the relationship to the surface of the head (*i.e.*, the interface with the environment), including a prediction for the position of an echolocation beam emanating from the head; and (3) the likelihood that specific frequencies (wavelengths) could be propagated and/or refracted through the melon based on the dimensions of potential pathways.

In order to describe the topography of density within the melon, we tabulated the mean, standard deviation, maximum, and minimum HU values for the entire melon. These statistics for the HU values in the melon provided a measure of organ homogeneity (*i.e.,* narrow range and low standard deviation indicates a more homogenous density within the melon and *vice versa*). The organization of the density topography within the melon provided a qualitative descriptor of melon structure. We examined the topography of melon density using images with a color spectrum spread across the various densities within the melon (where red represents the low density end of the spectrum and green represents the high density end of the spectrum). This technique allowed us to characterize the topography of the density changes across the melon, making particularly apparent the low density core (see Fig. 3).

The volume of melon was estimated by summing all of the 3-D volume elements (voxels) that make up the melon in each slice; the voxels are cubic, so the volume is equal to the cube of length, in this case, the thickness of the slice. In order to control for the effects of scale, considering the large size range of the species in this study, the volume (size) of the melon was presented as the percent of the total volume of the head. The volume of the head was defined by the boundary at the skin over the entire head, from the tip of the rostrum to the occipital condyles (condylobasal length). We also measured the maximum length of the melon and compared it to the condylobasal length as another indicator of relative size.

The geometric relationship of the melon to other forehead structures was based on the Cartesian coordinate information contained in the scans. The CT scanning process provided detailed locations within the specimen by x (dorsal–ventral position), y (right–left position), and z (anterior–posterior position) coordinate values; we used these values to measure distances between various structures of interest. We measured the width of the interface between the melon and the surface of the head (see Fig. 4 *Tursiops* for visualization of the measurement), reasoning that this region minimizes the impedance mismatch across the tissue-water interface, and likely facilitates transmission of the highest intensity pathway for echolocation clicks exiting the head, as suggested by Cranford *et al.* (2008*a*) and Au *et al.* (2006). Furthermore, the dimensions of this region might restrict the wavelengths (frequencies) that could be efficiently propagated through this interface. For example, if the region is smaller than the wavelength of sound (as defined by a particular frequency) that sound will tend not to propagate through that aperture. Another measurement was the distance from the posterior melon to the right and left bursae. Previous studies described the qualitative and quantitative attachment between the melon and the bursae complexes for a number of specimens (Cranford *et al.* 1996, Harper *et al.* 2008) and we provide these descriptions for additional species.

Qualitative descriptions of melon shape include descriptors of its overall shape (*i.e.,* elliptical, or dorsal–ventral flattened, or box-like, noting any extensions or modifications, particularly posterior extensions that project toward the sound generation structures. When describing melon shape, we refer to different regions of the melon but it was difficult to define these regions as homologous because the configuration of the underlying bony basement varied considerably across odontocetes. Instead,

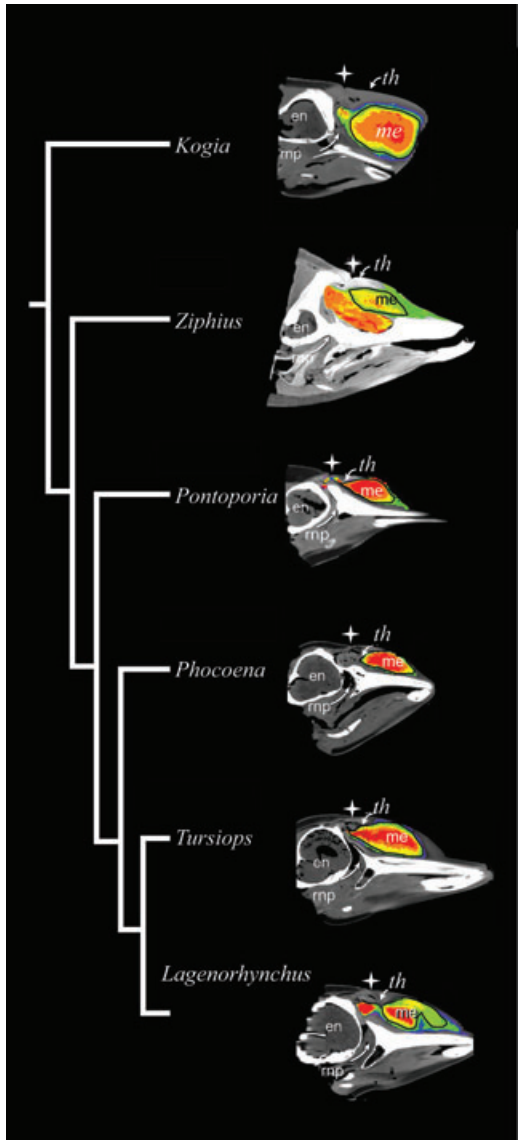

Figure 3. Two-dimensional parasagital views represent CT scan sections (density maps) from different odontocete species, arranged phylogenetically. The scan sections are through the head slightly to the right of the midline, capturing the right nasal passage. From top down, representative odontocetes include *K. breviceps*, *Z. cavirostris* (adult), *P. blainvillei*, *P. phocoena*, *T. truncatus*, and *L. obliquidens*. The color in the images represents the density of internal melon anatomy: white (bone), gray (soft tissue), blue (dense connective tissue) high density, green, yellow and orange the melon, and red (melon core) low density. The boundaries of the melon are outlined in black. Abbreviations: en = endocranium, me = melon, rnp = right nasal passage, th = theca indicated by arrow. White stars denote the position of the external blowholes. Note the *Kogia* skull is canted downward to be consistent with the articulation of the vertebral column with the skull.

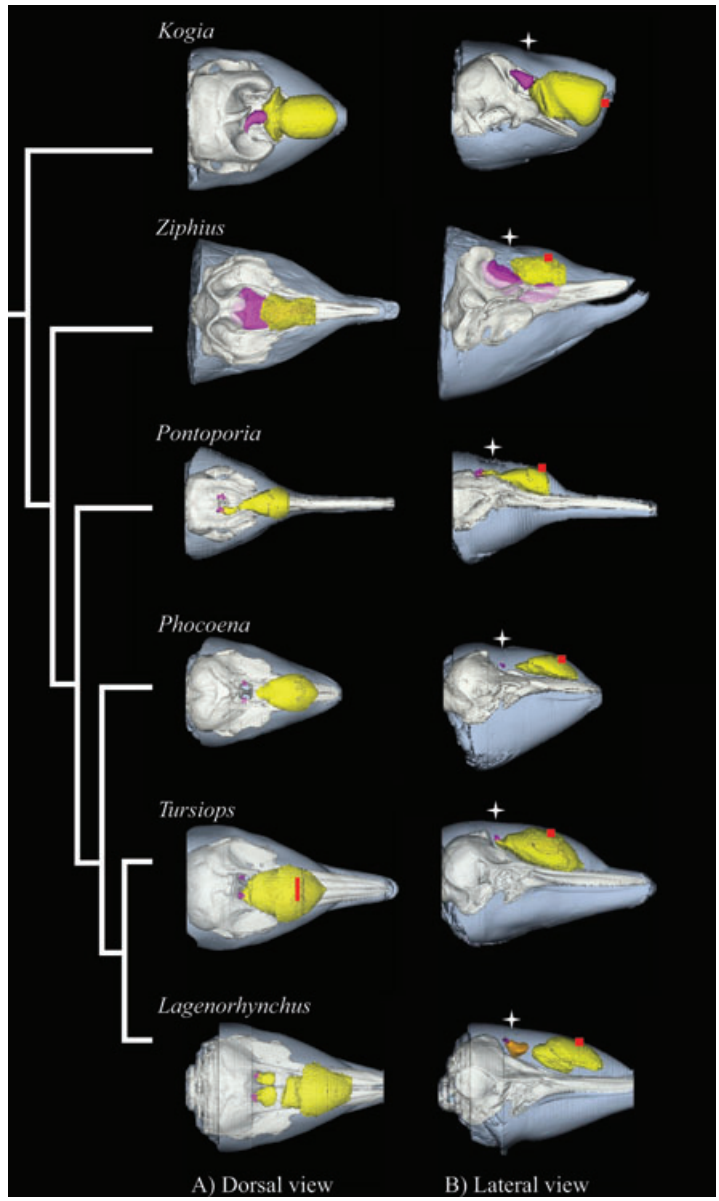

Figure 4. Three-dimensional reconstructions of melon morphology from different odontocete species, arranged phylogenetically. From top down, representative odontocetes include *K. breviceps*, *Z. cavirostris* (adult), *P. blainvillei*, *P. phocoena*, *T. truncatus*, and *L. obliquidens*. In (A) 3D dorsal views and (B) 3D lateral views, colored structures represent: gray = skin, white = skull, yellow = melon, magenta = bursae complexes or spermaceti organ, orange = fat bodies. *Tursiops* shows the measurements of the width of the connection of the melon to the surface of the forehead (red line in A). In the lateral views (B), the white stars denote external blowhole and red squares indicate the predicted region of an echolocation click exiting the head.

we generally refer to components relative to fractions along the melon's length: the anterior melon was the anterior fourth of the melon; the posterior melon was the posterior fourth; and the main body, which is the bulk of the melon, was the remaining middle section of the melon.

RESULTS

Descriptions of the melon are presented for each odontocete Family, including a discussion of melon morphology, comparisons with other taxa, and summaries of the quantitative comparisons for each morphological feature.

Kogiidae

Many of the morphological features within the forehead of the pygmy sperm whale (*K. breviceps*)($n = 2$, both juvenile specimens) are common to the Physeteridae (Cranford 1999). The sperm whales exhibit the most extreme deviation in the bone and soft tissue nasal anatomy when compared to all other odontocetes (Fig. 3, 4). The HU values indicate that the melon in the pygmy sperm whale is encased in a thick layer of connective tissue and blubber on its dorsal and lateral borders, similar to that described by Clarke (2003) for *Kogia* and Harper *et al.* (2008) for *Tursiops*. There is also a distinct topography within the melon of *K. breviceps*, as seen in the highly organized gradation in density changes, shown in color in Fig. 3: the low density core (red), surrounded by progressively higher density regions (orange, yellow, and green). These density regions are distinct, close together, and continuous within the melon, except at the anterior melon where the lower density regions come close to the surface of the head. Compared with the other species in this study, the two juvenile *K. breviceps* specimens showed the most highly organized and distinct gradation in density regions within the melon (Fig. 3).

In *K. breviceps*, the posterior melon directly abuts the spermaceti organ (Fig. 4A). Lateral wing-like projections extend from the posterior melon (Fig. 4A). The anterior region of the melon follows the external contour of the forehead. The bulbous main body of the melon, the posterolateral extensions, and anterior anatomy all combine into a unique melon shape in *K. breviceps*. The melon is closest to the surface along its anterior border in a region that is roughly half of the width (2.4 cm) of the anterior surface of the forehead. The melon protrudes beyond the rostrum of the skull, which is canted downward at an angle of approximately 20° from the horizontal plane of the body (see Fig. 3). This is the same downward angle reported for the sperm whale (*Physeter catodon*) by Cranford (1999).

Ziphiidae

We examined the forehead anatomy of Cuvier's beaked whale (*Z. cavirostris*; $n = 2$, an adult male and a neonate female specimen). In the neonate specimen, the anterior boundary of the melon is not distinct, as the density diffuses into the adjacent tissues. The posterior melon is distinctive from the surrounding tissue and appears as narrowing channels extending posteriorly. Similar morphological features were observed in other neonate and juvenile beaked whale specimens (*Mesoplodon densirostris* and *Mesoplodon peruvianus*). The remaining *Ziphius* description will focus on the adult male specimen because melon development is likely incomplete in

neonates, and as a consequence, melon morphology and the moieties of acoustic fats (Koopman *et al.* 2003, Zahorodny-Duggan *et al.* 2009) cannot provide consistent or valid comparisons. For a description of the variation in neonate *Ziphius* melon morphology, see Cranford *et al.* (2008*b*).

Although the features of the dorsal aspect of the ziphiid skull cannot be considered as extreme as they are in sperm whales, there are some noteworthy features in the forehead soft tissue in the ziphiid specimens analyzed here. The fatty structures in the forehead of the adult male *Ziphius* formed two distinct bodies: (1) a dorsal region that extends anteriorly along the rostrum (the melon); and (2) a lower density structure nestled in a bony basin (*i.e.*, the prenarial basin described by Heyning 1989), formed by the premaxillae, maxillae, and vomer (Fig. 4). Although this lower density fat body was thought by Norris and Harvey (1972) to be homologous to the spermaceti organ in sperm whales, Cranford *et al.* (2008*b*) proposed the term "anterior spermaceti organ" for this structure in *Ziphius* because its anatomic relationship with the spiracular cavity was not the same as the right nasal passage and the spermaceti organ in sperm whales. In addition, the sound production anatomy of ziphiids is apparently inverted dorsoventrally compared to sperm whales. In *Ziphius* the melon is dorsal to the anterior spermaceti organ, unlike sperm whales where the melon homologue (junk) is ventral to the spermaceti organ (see Cranford 1999, Cranford *et al.* 2008*b*). The anterior spermaceti organ in the adult *Ziphius* extends posteriorly in two branches to a region dorsal to the right bony nasal passage; the right branch twice the width of the left (in Fig. 4 ventral to the apex of the skull). In the male *Ziphius*, the anterior terminus of the anterior spermaceti organ ends abruptly at an interface with an extremely dense bone, the vomer (Fig. 3, 4).

The melon in the adult *Ziphius* is connected to the middle section of the anterior spermaceti organ, and extends anteriorly towards the surface of the forehead (Fig. 4B). The shape of the melon is box-like, and the anterior terminus of the melon ends bluntly approximately half way along the rostrum. The melon is closest to the surface of the forehead approximately two-thirds along its length anteriorly. The melon is distinct from the surrounding tissue, especially on the dorsal and lateral surfaces; however, there was a lack of highly organized or distinct topography (as represented by density gradients) within the melon (Fig. 3). This stands in stark contrast to the melon in *K. breviceps*.

Pontoporiidae

Only one of the "river dolphin" lineages, Pontoporiidae, was represented in this study by the franciscana (*P. blainvillei*). The anterior boundary of the melon had a relatively broad and flattened surface, similar to that of the adult *Ziphius* (Fig. 4B). The main body of the melon was bulbous in shape and had a distinct lower density core (Fig. 3). The posterior melon extends in a right branch, which connects directly with the right bursae complex, an elongate pathway that twists (along 34% of total melon length) in a left-hand corkscrew-like pathway, when viewed from an anterior to posterior orientation (Fig. 4A) (Cranford *et al.* 1996, Huggenberger *et al.* 2010). There is a discontinuity in the pathway between the main body of the melon and the left dorsal bursae complex in *Pontoporia*. This discontinuity can be seen as a short gap (~2 cm) in the low density pathway. The melon runs closest to the surface of the forehead along the anterior-most region of the melon (Fig. 4).

Phocoenidae

In *P. phocoena*, the only phocoenid analyzed in this study, the main body of the melon is dorsoventrally flattened (Fig. 4). Although a low density core is present, the gradient to the surrounding melon is steeper, as compared to *Kogia*, *Tursiops*, and *Delphinus.* The lateral aspects of the melon are bounded by connective tissue and the dorsal surface of the anterior melon closely approximates the surface of the forehead (Fig. 4). Unique to *Phocoena,* the posterior melon tapers to a point (Fig. 4B) and ends near the midline of the skull, just anterior to the bony nasal passages (Cranford *et al.* 1996, Huggenberger *et al.* 2009). There is no direct contact with either the right or left bursae complexes, complexes that are located equidistant (21.5 mm) from the midline of the skull and 26 mm from the posterior tip of the melon. The result is that there is a density discontinuity between the posterior melon and both bursae complexes.

Delphinidae

The Delphinidae is the most speciose group within the Odontoceti, represented in this study by five species: *T. truncatus* ($n = 3$ adults), *D. delphis* ($n = 2$ adults), *O. orca* ($n = 1$ adult), *S. bredanensis* ($n = 1$ adult) and *L. obliquidens* ($n = 1$ subadult and 1 adult). All of the delphinids share similar external head morphology, including a gently sloping forehead and the presence of a beak (some shorter than others); although the internal anatomy exhibits greater diversity than might be suggested by the external morphology.

The size of the melon relative to the head size varied among delphinids. The melon in *Orcinus* was only 2% of the total head volume, compared to 3%–4% of total head volume in *Tursiops* and *Delphinus* (Table 1); however, the melon in the *Orcinus* is at least seven times larger (in absolute terms) than the *Tursiops* melon. The head of *Orcinus* is more than 22 times larger (in absolute terms) than the head of the *Tursiops* specimen (this is also borne out in Table 1). Most of the variation within the delphinid melon was found in the posterior and anterior regions. The main body in all species was ovoid (Fig. 4), with a distinct lower density core (Fig. 3). The posterior and anterior regions were anchored in the connective tissues of the forehead; however, the dorsal surface of the main body of the melon closely approximated the surface of the forehead in all delphinid species analyzed, except *Orcinus*. In *Orcinus*, the main body of the melon remained buried deep to the surface layers of tissue and appeared dorsoventrally flattened.

By our definition, the anterior region of melon in *Tursiops*, *Delphinus*, *Steno*, and *Orcinus* became diffuse and graded into the surrounding tissues approximately midway along the bony rostrum; in *Lagenorhynchus* the melon extended further anteriorly. We noted an interesting difference between the anterior region and the melon core. In *Tursiops*, *Delphinus, Steno,* and *Orcinus* the melon core extended into the anterior region of the melon, but in *Lagenorhynchus* the core seems to terminate abruptly in the main body of the melon (Fig. 3). In *Lagenorhynchus*, the ventral surface of the main body of the melon was invaded by a transverse, connective tissue post (as described in Cranford *et al.* 1996), just anterior to the end of the melon core (Fig. 3). The prevalence of this post across the Delphinidae is unknown, but it was not observed in any of the other delphinids investigated here.

The posterior region of the melon in *Tursiops*, *Delphinus, Steno,* and *Orcinus*, extends from the right side of the main body and connects directly to the right burse complex,

as described by Cranford *et al*. (1996) and Harper *et al.* (2008) for *Tursiops.* In these delphinids there is a discontinuity in the low density pathway between the melon and the left bursae complex. In *Lagenorhynchus*, the relationship between the melon and the bursae complexes is unique, as compared to all other species analyzed (Fig. 4). The posterior melon in *Lagenorhynchus* extends in two similar sized channels, where the density increases slightly (Fig. 3), toward the left and right bursae complexes. Just anterior to the bursae complexes, each branch expands into a lipid basin shaped like an upside-down pyramid (Cranford *et al*. 1996) and each extension connects directly to the respective right and left bursal complexes (Fig. 3).

Morphometric Comparisons of the Melon

In this section, anatomic descriptions and quantitative measurements for the different morphological characters of the melon are compared.

The relationship between melon size and head size is curious. Generally, melon size appears to increase with head size, (Table 1); however, this trend is not isometric because the melons of *Orcinus* and *Steno* are smaller than expected, as a percentage of head volume. The neonate female *Ziphius* has a melon that is nearly twice the size of the adult male *Ziphius* melon, as a percentage of head volume. At this point, we cannot say whether the difference in the size of the melon between the two Ziphius specimens is due to differences in allometric growth or sex or both.

The anterior structure of the melon core varied across odontocetes (Fig. 4B). In *Tursiops, Delphinus, Steno, Orcinus,* and *Phocoena*, the melon core tapered to a rounded anterior terminus above the midline of the skull, similar to the main melon body. In *Kogia*, *Lagenorhynchus, Pontoporia*, and *Ziphius* the anterior melon core ended somewhat abruptly by comparison and blunt in appearance.

The density of the melon was described using the mean HU value of the melon. *Tursiops* and *Kogia* had the lowest average HU values or lowest densities (−91 to −81 HU). *Pontoporia* and *Phocoena* had mean HU levels between −75 and −66 HU (see Table 1). The highest mean densities were found in *Steno, Lagenorhynchus, Delphinus,* and *Ziphius* (neonate) (greater than 58 HU).

The difference between the maximum and minimum HU values was used to describe the internal range of variation in the density of the melon (see Table 1). *Steno* had relatively little variation (most homogeneous) in melon density (6 HU). *Lagenorhynchus, Phocoena, Tursiops, Kogia, Ziphius* (neonate), and *Delphinus* displayed intermediate levels of variation (50–94 HU). *Pontoporia* exhibited extreme variation in HU values (169 HU).

We quantified the internal structure of the melon based on how different densities were organized within the melon, using a color map (Fig. 3). The internal structure showed different characteristics across the specimens. In *Kogia* we found a gradual density gradient that is seen as concentric density regions (*i.e.,* a constant slope in density change) in Fig. 3. In *Tursiops*, *Phocoena*, and *Lagenorhynchus* there is a steep gradient at the boundary of the outer shell and a distinct low density core and outer shell, without an obvious gradation in density. In some cases, the relationships between density regions appear to be less distinct, particularly in the neonate specimens (*i.e., Ziphius* neonate and adult), or with low density differentiation (*Steno*).

Ziphius (adult) had the greatest melon width at the surface of the head (aperture), and *Pontoporia, Steno, Phocoena*, and *Kogia* had the smallest region of direct connection between the melon and the surface of the head (Table 1). The width varied within delphinids (2.5–22.9 cm).

The low density connections between the melon and the bursae complexes varied. Most often, there was a continuous connection between the right posterior extension of the melon and the right bursae complex (*e.g.*, *Tursiops*, *Delphinus*, and *Pontoporia*); these species and the other delphinids we have examined also have a left posterior extension of the melon although, as previously noted, the pathway contains a gap or density discontinuity along the pathway to the left bursae complex (Cranford *et al.* 1996). In *Ziphius* the posterior melon ends bluntly but connects ventrally to the anterior spermaceti organ that bifurcates into left and right branches posteriorly (Cranford *et al.* 2008*b*). In *Kogia*, the posterior melon also ends in a blunt rounded protrusion that abuts to the enlarged end of the J-shaped spermaceti organ (Fig. 4). The posterior melon does not bifurcate in *Phocoena*, rather it tapers to a point and terminates dorsal to the premaxillary eminences of the skull, immediately anterior to the bony nasal passages. We observed a unique structural configuration in the *Lagenorhynchus* posterior melon leading to the bursae complexes. The posterior melon extends toward both bursae complexes and then connects to the two fatty basins immediately before arriving at, and connecting directly to the right and left burse complexes respectively, as described by Cranford *et al.* (1996) and shown in Fig. 3 as the orange fat bodies.

Discussion

Functional morphology in organisms is based on understanding the inseparable connection between structure and function (Wainwright 1988). Here we report on the structure of the odontocete melon across a broad spectrum of extant odontocetes in an effort to extrapolate to a more complete understanding of melon functional morphology. We created a standardized definition for the melon boundaries using the density gradients gleaned from CT scan data. This approach allowed us to investigate melon morphology without sacrificing its geometric integrity and make comparisons of structure between odontocete species.

Odontocete forehead lipids have been implicated as acoustic tissues, thought to focus the echolocation sounds and perform an impedance matching function (Norris 1964, 1968; Norris and Harvey 1972; Mead 1975; Malins and Varanasi 1975; Au 1993). These fatty forehead tissues are roughly impedance-matched to sea water, as Norris and Harvey (1974) first elucidated; providing an efficient means of transmitting sound across the tissue-water interface. Simulations with Finite Element Models (FEM) demonstrated that the melon in *Ziphius* is capable of some focusing in the formation of an echolocation beam from a click produced at the location of the phonic lips (Cranford *et al*. 2008*a*). Prior studies on the chemical and physical analysis of the lipids that comprise the melon provide a molecular basis for the role of shaping the sound beam (Varanasi and Malins 1971, 1972; Varanasi *et al.* 1975; Karol *et al*. 1978; Clarke 1970, 2003; Norris and Harvey 1974; Litchfield *et al.* 1979; Goold and Clarke 2000; Koopman *et al.* 2003). Furthermore, these unique lipids represent a large energy investment that may not be recoverable because these lipids apparently cannot be used metabolically when normal energy reserves are low, suggesting that these fats serve another function.

Below we consider how melon morphology might relate to acoustic function (*i.e.,* the focusing of echolocation sounds and the pathways these sounds travel in the forehead). Acoustic functions of the melon have previously been investigated in

some odontocete species (Norris *et al*. 1961; Evans *et al*. 1964; Schevill and Watkins 1966; Evans 1973; Norris and Harvey 1974; Carvan 1988; Møhl *et al*. 2000; Au *et al*. 1986, 1999, 2006, 2010). We will discuss our results in light of this previous work and consider an additional acoustic function for the melon, that of establishing a lower frequency limit for sounds that can propagate through it. We acknowledge that extracting function from structure is a perilous undertaking that can result in simplistic views of complex and often subtle processes. In this case, it is an initial step in understanding.

Focusing Capability of Melon

The primary acoustic function of the melon may be its ability to focus sound, thereby amplifying components of the outgoing signal (Norris and Harvey 1974). It is reasonable to predict that several facets of melon structure and the adjacent structures are important in the resulting function. Clearly the molecular structure of the various lipids (Malins and Varanasi 1975), their topographic distribution (Litchfield *et al.* 1979, Koopman *et al*. 2003), and the juxtaposition of tissue interfaces (air spaces and dense connective tissue) with vastly different acoustic impedance values, all combine into a synergistic and finely tuned function. Any of these structures alone are unlikely to have a significant functional influence, except perhaps the air spaces. The single most important functional characteristic is the speed of sound in biological tissue, which depends on the density and elasticity of the conducting and adjacent tissues (Duck 1990). Sound bends or refracts towards lower density (*i.e.*, lower sound speed) as it propagates, in all but specialized conditions (Blackstock 2000). Consequently, sagittal profiles of the density changes in the melon provide useful information that bears on sound refraction within the melon (Fig. 3).

Kogia displayed the most organized density gradients within the melon, the highest density near the external surface grading to a low density core (Fig. 3). This intricate density topography is not visible in anatomic sections (see, *e.g.*, Fig. 2, 3, and 5 in Clarke 2003). *Kogia* also exhibited more variability in HU values and the lowest observed densities (Table 1). This density topography may be related to differences in the lipid composition. Karol *et al*. (1978) found three regions of distinctive lipid composition in *Kogia*: (1) a fat-poor melon exterior, similar to the higher density outer layer observed in this study; (2) an outer melon of medium fat content having more triglyceride present compared to wax esters; and (3) a fat-rich "inner melon" with more wax esters present compared to triglycerides, likely similar to the low density melon core found in this study. The lowest observed HU values in the *Kogia* melon core likely correlate with the presence of lower density wax esters. It is possible that the gradual progression to a low density core found in the *Kogia* melon enhances the focusing or narrowing of the echolocation beam, compared to delphinids. The capability to focus sound using compositional topography of the melon lipids may be particularly useful in the deep diving odontocetes, which will have a limited air volume at depth due to hydrostatic pressure, and consequently only limited contribution to focusing by reflection from air sacs. Instead, some acoustically reflective functions in deep diving species, like *Kogia* and *Ziphius*, are likely accomplished by interfaces between lipids and dense connective tissue and/or bone. In *Kogia,* the phonic lips that expel air into the central depression of a curious multilayered structure are located at the posterior terminus of the spermaceti organ. This structure, variously named (Schenkkan and Purves 1973, Cranford *et al.* 1996,

Clarke 2003), resembles a bird's nest and is composed of alternating paraboloid layers, thick dense connective tissue layers alternating with thin layers of filigreed air spaces. The air space layers are part of the right nasal passage and resemble a catacomb-like structure, a series of interconnected passageways with small niches or chambers leading off them.

Another feature of the melon that may enhance its focusing capacity is length; the longer the lipid pathway for sound, the greater the distance over which the sound could be focused. Sperm whales exemplify this idea (Cranford 1999), with folded lipid pathways that may be twice the length of the forehead, a continuous pathway that includes both the melon and the spermaceti organ. In this study, *Kogia* had the longest melon relative to head size (60%; Table 1), and when the spermaceti organ is included, the combined length is significantly longer than all other species, suggesting potential for superior focusing capacity. In deep diving odontocete species, like *Kogia,* dense connective tissue may act as a substitute for air spaces in an acoustically reflective function, as discussed earlier (Cranford *et al.* 1996, 2008*b*). Increased melon length, dense connective tissue boundaries, and compositional lipid topography in the Physeteridae may add up to significant acoustic focusing.

Propagating acoustic waves in the head will also be influenced by ancillary structures, such as those adjacent to the melon and presumably the details of melon shape. Unique shapes of the melon found in different species may provide some clues as to how signals might vary based on the gross differences in melon shape and any nearby appendages. For example, *Kogia* has unique wing-like structures that extended laterally from the posterior melon (Fig. 3). Within the Delphinidae, the main body of the melons have a similar oval shape, but the posterior and anterior regions differ. *Lagenorhynchus* had a blunt anterior surface to the melon core, unlike the tapered appearance in *Delphinus* and *Tursiops* (Fig. 3, 4). There are vast differences in the types of signals produced by pygmy sperm whales and many modern delphinids. For example, *Tursiops* produces a brief (50 μs) oligocyclic signal and has two sets of phonic lips (the likely sonar signal generators), whereas *Kogia* produces a longer (150 μs) polycyclic signals from a single set of phonic lips. These complex differences in signal type may be, at least partially, a function of the complex differences in melon morphology but it is difficult to evaluate or to assign specific functions to various shapes or appendages. Computer models and simulations might provide some insight into the various functional aspects of melon shape.

An important component to the pathways of sound in the head is the relationship between the melon and the sound source(s) (*i.e.,* phonic lips or *museau du singe*, dorsal bursae, and the spermaceti organ) (Cranford *et al.* 1996, 2008*a*). In odontocetes, sound is thought to radiate from a specific source(s) (Cranford *et al.*, in press) and therefore the source position relative to the melon is a critical component in understanding how sound propagates in the head. The attachment of the melon to the bursae complexes varies across the odontocete species, as seen in this study and previous morphological studies (Cranford *et al.* 1996, 2008*b*). All delphinid species were similar in that the right posterior extension of the melon is continuous and attaches directly to the right bursae complex, while the left posterior extension of the melon always contained a discontinuity in the pathway to the left bursae complex. *Lagenorhynchus* was the only exception. In the Pacific white-sided dolphin, the posterior melon bifurcates into right and left branches that each expand into upside down pyramidal fatty basins just before reaching their respective bursae complex (Fig. 4). Although the precise functions of these morphological features are unknown, they likely play a role

in the shaping the outgoing echolocation signal. One possible mechanism is that constructive and/or destructive interference act to partially shape the biosonar signal within the complex acoustic environment of the odontocete forehead, a process that likely begins with sound generation events at one or both bursal complexes (Lilly 1962; Evans 1973; Cranford *et al.*, in press). Further experimental research is needed to test this function. Delphinid echolocation signals tend to be broad band clicks (30–150 kHz), but the spectral structure of the clicks vary within the group (Soldevilla *et al.* 2008) and can vary within individuals (Au *et al*. 1995). There is a consistent and distinctive spectral peak and notch structure present in *Lagenorhynchus* and *Grampus* echolocation signals, but not in *Tursiops* and *Delphinus* signals (Soldevilla *et al.* 2008), possibly related to differences in melon bursae connection.

Models of the echolocation systems within delphinids may help determine if the relationship between the bursae and melon influences the click structure by filtering, focusing, or another mechanism, as a result of the combined geometric and density relationships between structures. *Kogia* and *Phocoena* have similar echolocation signals (long duration, narrow bandwidth signals above 100 kHz) (Madsen *et al.* 2005) despite a major difference between their bursae-melon connections. This finding suggested that similar signals can be produced by different sound generation mechanisms, sound pathway morphologies, and short term temporal changes such as building air pressure or maintaining tension on vibratory components. If the nonphyseteroid odontocetes possess at least two independent sound sources (*i.e.*, right and left bursae), as suggested by Cranford and others (Cranford and Amundin 2000; Cranford *et al.*, 1996, 2008*a*; Lammers and Castellote 2009; Cranford *et al.*, in press), it is possible that constructive and/or destructive interference could produce overlapping sonar beams just outside the head that would reveal the nature of the relationship between the melon and both potential sources. Unearthing the nature of this relationship is essential for guiding future investigations into the functional morphology of odontocete biosonar.

It is evident that the relationships between melon morphology (*i.e.,* density structure, length, shape, and connection to bursae) and acoustic function (focusing, filtering, and impedance matching) are complex. This complexity is not surprising given that the production of clicks involves the manipulation of many structures, often within fractions of a second. Harper *et al.* (2008) suggested that the complex connective tissues and muscles acting on the melon allow for active manipulation of melon shape in *Tursiops*, implying *in vivo* adjustments to sound characteristics are possible. Since all odontocetes apparently have muscle and connective tissue connections to the melon, we assume that this "active manipulation" idea can be extrapolated to include the entire clade and may be a factor in beam steering. Across all the species analyzed in this study, we observed the same general connective tissues structure surrounding the melon, with increasing density gradients. The orientation of the connective tissue fibers was not possible to distinguish using CT imaging, making it difficult to characterize or quantify how different odontocetes could modify melon shape with connective tissue fibers and muscle.

Frequency Filtering by the Melon

Another possible acoustic function that may be associated with melon morphology is the facility to limit signal frequency, although the size and shape of each bursae complex are undoubtedly important components in determining the frequency

composition of generated signals (Cranford *et al.* 1996). The diameter of the melon might act to restrict or "filter out" low frequencies with wavelengths longer than melon cross-sectional dimensions. This would prevent the melon from acting as a waveguide for these long wavelength sounds, thereby providing a predictable lower limit on the frequency of the sounds that can be propagated through the melon. Smaller diameter melons could further constrain the size of the waveguide and restrict concomitant wavelength sounds (*i.e.,* lower frequencies) from being propagated through the melon, essentially functioning as a low frequency "noise" filter.

Melon diameter will not predict the exact frequency composition of biosonar signals because the process of generating a signal, filtering or amplifying it, and forming it into a sonar beam is a complex process involving the action of a number of anatomic components working in concert. Perhaps the most useful quantity measured in this study is the width of the melon or "aperture," where the low density melon tissue reaches closest to the interface between the head and the environment. This feature was first described for *T. truncatus* by Norris and Harvey (1974), and designated as the area with the best impedance match to the surrounding water. Au *et al*. (2006) demonstrated that this region is where the highest intensity echolocation beam exits the head in *P. phocoena*.

The dimensions of this region may be important for determining the frequency of the acoustic signal that can pass through this aperture, that is, a smaller aperture size would set the lower limit for the wavelength that can be propagated out of the head. For example, the width of the melon at the surface of the head in the adult *Tursiops* was 5–6 cm (Table 1), which (assuming 1,500 m/s speed of sound in the medium) translates to a minimum frequency of 25–29 kHz, compared to an estimated minimum frequency of 40 kHz in the harbor porpoise. This relationship might not hold for narrow band echolocation clicks if the bandwidth limit is larger than the frequency emphasis in the signal. For example, *Ziphius* and *Phocoena* produce narrow band clicks (38–60 kHz from *Ziphius* compared to 120–140 kHz from *Phocoena*) (Cranford and Amundin 2004, Johnson *et al.* 2004, Baumann-Pickering *et al*. 2010), therefore we may not expect to see the effects of selective pressure on the low frequency limit based on aperture size, since the wavelength in *Phocoena* is much smaller than the aperture size. As another example of the functional significance of the aperture, consider a comparison between *Kogia* and *Phocoena*. The highest recorded frequencies have been observed in both *Phocoena* and *Kogia*, yet they exhibit substantial differences in melon size, sound source dimensions, and melon anatomy. One possible explanation for the similar echolocation signal is a similar sized melon aperture functioning to filter out lower frequencies (Table 1). One possible biological advantage of filtering out lower frequencies, which propagate longer distances underwater, is that acoustic signals will be less likely to be overheard by predators.

Although specific melon morphologies will influence resulting acoustic signals, the geometric details of the entire echolocation system components need to be considered when interpreting how melon structure relates to acoustic function. For example, in computer simulations, Aroyan *et al.* (1992) found that moving the sound source just a few millimeters significantly changed the direction, intensity, and frequency of the resultant beam. Computer modeling techniques like FEM have revealed a mechanism by which the melon and associated cranial structures (*e.g.,* pachyosclerotic elements of the skull) could contribute to beam focusing or condition the outgoing signal in *Ziphius* (Cranford *et al.* 2008*a*). Both computer simulation studies suggest that

tissue geometry may have a greater influence on the beam formation than actual tissue properties. Furthermore, the production of echolocation clicks is an active process and can be modified *in vivo*. Descriptions of the musculature and connective tissues surrounding the melon suggest that odontocetes may have the ability to actively modify sound propagation in soft tissue structures (Mead 1975, Moore *et al.* 2008, Harper *et al.* 2008). It is also worth noting the relationship of melon morphology and the external shape and contour of the forehead and the consequences for the hydrodynamic constraints related to swimming performance (Fish 1998, Ridgway and Carter 1993). Separating these hydrodynamic relationships from acoustic function and the consequences for the internal anatomy of the odontocete forehead is nontrivial and beyond the purview of this study.

Conclusion

Differences in melon size, shape, and position within the heads of nearly all odontocete families, provide insight into which features might produce the recorded variation in echolocation signals. The use of *in situ* CT scanning proved to be a powerful tool to investigate the melon without disrupting the geometric integrity of the structure and its relationship to the overall forehead anatomy; such investigatory tools are important because a precise understanding of relationships among individual components of the odontocete forehead are necessary to decipher bioacoustic function. Using CT scanning does not obviate the need for detailed anatomical investigation using traditional means, but rather its associated tools and techniques complement and provide investigators with the unique flexibility to view the anatomic structures from any angle, color, opacity, or configuration, and at any time, with little or no specimen preparation required. The results of our study may be valuable when making interpretations of differences in echolocation signals and designing theoretical models to understand the mechanisms behind echolocation beam formation. Furthermore, the morphological characters provide the necessary material to examine the evolution of specific echolocation capabilities in odontocetes.

Acknowledgments

The work described here was completed in partial fulfillment of a Master's of Science degree by the senior author in the Department of Biology at San Diego State University. Many to thanks to those who provided the specimens used in this study, including: S. Chivers, K. Danil, J. Heyning, J. St. Leger, S. Ridgway, D. Duffield, S. Norman, S. Moore, and K. Balcomb. A special thanks to those involved in specimen preparation, scanning, and processing: C. Garsha, M. Stehler, J. Hildebrand, S. Wiggins, M. Soldevilla, M. Shaver, B. Heslop, A. McCarty, C. Lusk, S. Juares, R. Huber, K. Allen, T. Vanaberg, B. Campbell, D. Wicknam, J. Waterhouse, C. Ford, J. Knisely, S. Robinson, B. Gould, B. Knowles, R. Racicot, and M. Colbert. Thanks to J. A. Goldbogen for suggestions and inspiration to complete this work.

Some funding for this project came to M. F. McKenna from the San Diego State University Fund, ARCS Fellowship, Mabel Myer Scholarship, Smithsonian Institution's Remington Kellogg Fund, San Diego State University, Department of Biology, Evolutionary Biology Program Area. The most significant support for this research was provided to Dr. Ted W. Cranford by Dr. Robert Gisiner at the Office of Naval Research, and by Frank Stone and Ernie Young at the Chief of Naval Operations (CNO45).

Literature Cited

Au, W. W. L. 1993. The sonar of dolphins. Springer-Verlag Inc., New York, NY.

Au, W. W. L., P. W. B. Moore and D. Pawloski. 1986. Echolocation transmitting beam of the Atlantic bottlenose dolphin. Journal of the Acoustical Society of America 80: 688–691.

Au, W. W. L., J. L. Palowski, P. E. Nachtigall, M. Blonz and R. C. Gisiner. 1995. Echolocation signals and transmission beam pattern of a false killer whale (*Pseudorca crassidens*). Journal of the Acoustical Society of America 98:51–59.

Au, W. W. L., R. A. Kaskelein, T. Rippe and N. M. Schooneman. 1999. Transmission beam pattern and echolocation signals of a harbor porpoise (*Phocoena phocoena*). Journal of the Acoustical Society of America 106:3699–3705.

Au, W. W. L., R. A. Kastelein, K. J. Benoit-Bird, T. W. Cranford and M. F. McKenna. 2006. Acoustic radiation from the head of echolocating harbor porpoises (*Phocoena phocoena*). Journal of Experimental Biology 209:2726–2733.

Au, W. W. L., D. S. Houser, J. J. Finneran, W. J. Lee, L. A. Talmadge and P. W. Moore. 2010. The acoustic field on the forehead of echolocating Atlantic bottlenose dolphins (*Tursiops truncatus*). Journal of the Acoustical Society of America 128:1426–1434.

Amundin, M., and S. H. Andersen. 1983. Bony nares air pressure and nasal plug muscle activity during click production in the harbour porpoise, *Phocoena phocoena*, and the bottlenosed dolphin, *Tursiops truncatus*. Journal of Experimental Biology 105:275–282.

Aroyan, J. L., T. W. Cranford, J. Kent and K. S. Norris. 1992. Computer modeling of acoustic beam formation in *Delphinus delphis*. Journal of the Acoustical Society of America 92:2539–2545.

Baumann-Pickering, S., S. M. Wiggins, E. H. Roth, M. A. Roch, H. U. Schnitzler and J. A. Hildebrand. 2010. Echolocation signals of a beaked whale at Palmyra Atoll. Journal of the Acoustical Society of America 27:3790–3799.

Blackstock, D. T. 2000. Fundamentals of physical acoustics. Wiley, John and Sons, Inc., New York, NY.

Carvan, M. J. 1988. The descriptive anatomy of sound production and propagation tissues in *Kogia* spp. using magnetic resonance and computed tomography imaging. M.S. thesis, University of Miami, Coral Gables, FL. 72 pp.

Clarke, M. R. 1970. Function of the spermaceti organ of the sperm whale. Nature 228: 873–874.

Clarke, M. R. 2003. Production and control of sound by the small sperm whales, *Kogia breviceps* and *K. sima*, and their implications for other Cetacea. Journal of the Marine Biological Association of the United Kingdom 83:241–263.

Cranford, T. W. 1992. Functional morphology of the odontocete forehead: Implications for sound generation. Ph.D. dissertation, University of California, Santa Cruz, CA. 276 pp.

Cranford, T. W. 1999. The sperm whale nose: Sexual selection on a grand scale? Marine Mammal Science 15:1133–1157.

Cranford, T. W., and M. Amundin. 2004. Biosonar pulse production in odontocetes. Pages 27–35 *in* J. A. Thomas, C. F. Moss and M. Vater, eds. Echolocation in bats and dolphins. University of Chicago Press, Chicago, IL.

Cranford, T. W., M. Amundin and K. S. Norris. 1996. Functional morphology and homology in the odontocete nasal complex: Implications for sound generation. Journal of Morphology 228:223–285.

Cranford, T. W., P. Krysl and J. A. Hildebrand. 2008*a*. Acoustic pathways revealed: Simulated sound transmission and reception in Cuvier's beaked whale (*Ziphius cavirostris*). Bioinspiration & Biomimetics 3:1–10.

Cranford, T. W., M. F. McKenna, M. S. Soldevilla, *et al*. 2008*b*. Anatomic geometry of sound transmission and reception in Cuvier's beaked whale (*Ziphius cavirostris*). Anatomical Record 291:353–378.

Cranford, T. W., W. R. Elsberry, W. G. V. Bonn, *et al*. In press. Observation and analysis of sonar signal generation in the bottlenose dolphin (*Tursiops truncatus*): Evidence for two sonar sources. Journal of Experimental Marine Biology and Ecology. doi:10.1016/j.jembe.2011.07.010

Duck, F. A. 1990. Physical properties of tissue: A comprehensive reference book. Academic Press, San Diego, CA.

Evans, W. E. 1973. Echolocation by marine delphinids and one species of fresh-water dolphin. Journal of the Acoustical Society of America 54:191–199.

Evans, W. E., W. W. Sutherland and R. G. Beil. 1964. The directional characteristics of delphinid sounds. Pages 353–372 *in* W. N. Tavolga, ed. Marine bio-acoustics. Pergamon Press, New York, NY.

Fish, F. 1998. Comparative kinematics and hydrodynamic of odontocete cetaceans: Morphological and ecological correlate with swimming performance. Journal of Experimental Biology 201:2867–2877.

Fordyce, E., and C. de Muizon. 2001. Evolutionary history of cetaceans: A review. Pages 169–233 *in* M. Mazin and V. de Buffrenil, eds. Secondary adaptation of tetrapods to life in water. Verlag Dr. Friedrich Pfeil, Munich, Germany.

Gingerich, P. 2005. Cetacea. Pages 234–252 *in* K. D. Rose and J. D. Archibald, eds. The rise of placental mammals. John Hopkins University Press, Baltimore, MD.

Goold, J. C., and M. R. Clarke. 2000. Sound velocity in the head of the dwarf sperm whale, *Kogia sima*, with anatomical and functional discussion. Journal of the Marine Biological Association of the United Kingdom 80:535–542.

Griffin, D. R. 1980. Early history of research on echolocation. Pages 1–10 *in* R. G. Busnel and J. F. Fish, eds. Animal sonar systems. Plenum Publishing Corporation, New York, NY.

Harper, C. J., W. A. McLellan, S. A. Rommel, D. M. Gay, R. M. Dillaman and D. A. Pabst. 2008. Morphology of the melon and its tendinous connections to the facial muscles in bottlenose dolphins (*Tursiops truncatus*). Journal of Morphology 269:820–839.

Heyning, J. E. 1989. Comparative facial anatomy of beaked whales (Ziphiidae) and a systematic revision among the families of extant Odontoceti. Contributions in Science, Natural History Museum of Los Angles County 405:1–64.

Heyning, J. E., and J. C. Mead. 1990. Evolution of the nasal anatomy of Cetaceans. Pages 67–79 *in* J. Thomas and R. Kastelein, eds. Sensory abilities of cetaceans. Plenum Press, New York, NY.

Huggenberger, S., M. A. Rauschmann and H. H. A. Oelschläger. 2008. Functional morphology of the hyolaryngeal complex of the Harbor Porpoise (*Phocoena phocoena*): Implications for its role in sound production and respiration. The Anatomical Record 291:1262–1270.

Huggenberger, S., M. A. Rauschmann, T. J. Vogl and H. H. A. Oelschläger. 2009. Functional morphology of the nasal complex in the harbor porpoise (*Phocoena phocoena*). The Anatomical Record 292:902–920.

Huggenberger, S., T. J. Vogl and H. H. A. Oelschläger. 2010. Epicranial complex of the La Plata dolphin (*Pontoporia blanvillei*): Topographical and functional implications. Marine Mammal Science 26:471–481.

Johnson, M. P., P. T. Madsen, W. M. X. Zimmer, N. A. de Soto and P. L. Tyack. 2004. Beaked whales echolocate on prey. The Royal Society Biological Letters B 271:S383–S386.

Karol, R., C. Litchfield, D. K. Caldwell and M. C. Caldwell. 1978. Compositional topography of the melon and spermaceti organ lipids in the pygmy sperm whale *Kogia breviceps*: Implication for echolocation. Marine Biology 47:115–123.

Koopman, H. N., S. J. Iverson and A. J. Read. 2003. High concentrations of isovaleric acid in the fats of odontocetes: Variation and patterns of accumulation in blubber vs. stability in the melon. Journal of Comparative Physiology B 173:247–261.

Lammers, M. O., and M. Castellote. 2009. The beluga whale produces two pulses to form its sonar signal. Biology Letters 5:297–301.

Lawerence, B., and L. Schevill. 1956. The functional anatomy of the delphinid nose. Bulletin of the Museum of Comparative Zoology (Harvard) 114:103–151.

Lilly, J. C. 1962. Vocal behavior of bottlenose dolphin. Proceedings of the American Philosophical Society 106:520–529.

Lindberg, D. R., and N. D. Pyenson. 2007. Things that go bump in the night: Evolutionary interactions between cephalopods and cetaceans in the Tertiary. Lethaia 4:335–343.

Litchfield, C, R. Karol, M. E. Mullen, J. P. Dilger and B. Luthi. 1979. Physical factors influencing refraction of the echolocation sound beam in delphinid cetaceans. Marine Biology 52:285–290.

Madsen, P. T., D. Carder, K. Bedholm and S. H. Ridgway. 2005. Porpoise clicks from a sperm whale nose-convergent evolution of 130 kHz pulses in toothed whale sonars? Bioacoustics 15:195–206.

Malins, D. C., and U. Varanasi. 1975 Cetacean biosonar. Part II. The biochemistry of lipids in acoustic tissues. Pages 237–290 *in* D. C. Malins and J. R. Sargent, eds. Biochemical and biophysical perspective in marine biology. Volume 2. Academic Press, London,UK.

McKenna, M. F. 2005. Comparative morphology of the odontocete melon: Functional and evolutionary interpretations. M.S. thesis, San Diego State University, San Diego, CA. 211 pp.

McKenna, M. F., J. A. Goldbogen, J. St. Ledger, J. A. Hildebrand and T. W. Cranford. 2007. Evaluation of postmortem changes in tissue structure in the bottlenose dolphin (*Tursiops truncatus*). The Anatomical Record 290:1023–1032.

Mead, J. G. 1975. Anatomy of the external nasal passages and facial complex in the Delphinidae (Mammalia: Cetacea). Smithsonian Contributions to Zoology 207. 72 pp.

Mead, J. G., and E. R. Fordyce. 2009. The Therian skull: A Lexicon with emphasis on the odontocetes. Smithsonian Contributions to Zoology 627. 248 pp.

Møhl, B., M. Wahlberg, P. T. Madsen, L. A. Miller and A. Surlykke. 2000. Sperm whale clicks: Directionality and source level revisited. Journal of the Acoustical Society of America 107:638–648.

Moore, P. W., L. A. Dankiewicz and D. S. Houser. 2008. Beamwidth control and angular target detection in an echolocating bottlenose dolphin (*Tursiops truncatus*). Journal of the Acoustical Society of America 124:3324–3332.

Neuweiler, G. 2000. Biology of bats. Oxford University Press, New York. NY.

Norris, K. S. 1964. Some problems of echolocation in cetaceans. Pages 317–366 *in* W. N. Tavolga, ed. Marine bio-acoustics. Volume 1. Pergamon Press, New York, NY.

Norris, K. S. 1968. The evolution of acoustic mechanisms in odontocete cetaceans. Pages 297–324 *in* E. T. Drake, ed. Evolution and environment. Yale University Press, New Haven, CT.

Norris, K. S. 1969. The echolocation of marine mammals. Pages 391–423 *in* H. T. Andersen, ed. The biology of marine mammals. Academic Press New York, NY.

Norris, K. S., and G. W. Harvey. 1972. A theory for the function of the spermaceti organ of the sperm whale (*Physeter catodon* L.). Pages 397–417 *in* S. R. Galler, K. Schmidt-Koenig, G. J. Jacobs and R. E. Belleville, eds. Animal orientation and navigation. NASA Scientific and Technical Office, Washington, DC.

Norris, K. S., and G. W. Harvey. 1974. Sound transmission in the porpoise head. Journal of the Acoustical Society of America. 56:659–664.

Norris, K. S., J. H. Prescott, P. V. Asa-Dorian and P. Perkins. 1961. An experimental demonstration of echolocation behavior in the porpoise, *Tursiops truncatus* (*Montagu*). Biological Bulletin 120:163–176.

Ridgway, S., and D. A. Carder. 1993. Features of dolphin skin with potential hydrodynamic importance. IEEE Engineering in Medicine and Biology September:83–88.

Robb, R. A. 1999. Biomedical imaging, visualization and analysis. John Wiley & Sons, New York, NY.

Robb, R. A., and C. Barillot. 1989. Interactive display and analysis of 3-D medical images. IEEE Transactions on Medical Imaging 8:217–226.

Robb, R. A., D. P. Hanson, R. A. Karwoski, A. G. Larson, E. L. Workman and M. C. Stacy. 1989. ANALYZE: A comprehensive, operator-interactive software package for multidimensional medical image display and analysis. Computerized Medical Imaging and Graphics 13:433–454.

Schenkkan, E. J., and P. E. Purves. 1973. On the comparative anatomy and function of the nasal tract in odontocetes (Mammalia, Cetacea). Bijdragen tot de Dierkunde 43:127–159.

Schevill, W. E., and W. A. Watkins. 1966. Sound structure and directionality in *Orcinus* (killer whale). Zoologica 51:71–76.

Soldevilla, M. S., M. F. McKenna, S. M. Wiggins, R. E. Shadwick, T. W. Cranford and J. A. Hildebrand. 2005. Cuvier's beaked whale (*Ziphius cavirostris*) head tissues: Physical properties and CT imaging. Journal of Experimental Biology 208:2319–2332.

Soldevilla, M. S, E. E. Henderson, G. S. Campbell, M. Roch, S. M. Wiggins and J. A. Hildebrand. 2008. Classification of Risso's and Pacific white-sided dolphins using spectral properties of echolocation clicks. Journal of the Acoustical Society of America 124: 609–624.

Thomas, J. A., and M. S. Jalili. 2003. Echolocation in Insectivores and Rodents. Pages 547–564 *in* J. A. Thomas, C. F. Moss and M. Vater, eds. Echolocation in bats and dolphins. The University of Chicago Press, Chicago, IL.

Varanasi, U., and D. C. Malins. 1971. Unique lipids of the porpoise (*Tursiops gilli*): Differences in triacylglycerols and wax esters of acoustic (mandibular and melon) and blubber tissues. Biochimica et Biophysica Acta 231:415–418.

Varanasi, U., and D. C. Malins. 1972. Triacylglycerols characteristic of porpoise acoustic tissues: Molecular structure of diisovaleroylglycerides. Science 176:926–928.

Varanasi, U., H. R. Feldman and D. C. Malins. 1975. Molecular basis for formation of lipid sound lens in echolocating cetaceans. Nature 255:340–343.

Wainwright, S. A. 1988. Form and function in organisms. American Journal of Zoology 28:671–680.

Zahorodny-Duggan, Z. P., H. N. Koopman and S. M. Budge. 2009. Distribution and development of the highly specialized lipids in the sound reception systems of dolphins. Journal of Comparative Physiology B: Biochemical, Systemic, and Environmental Physiology 179:783–798.

Received: 6 May 2010
Accepted: 8 June 2011